Eur. Phys. J. D **29**, 285–292 (2004)
DOI: 10.1140/epjd/e2004-00030-6

THE EUROPEAN PHYSICAL JOURNAL D

A crisis of a stochastic web

Y.-M. Jiang[1,2], Y.-Q. Lu[2], X.-G. Chao[2], and D.-R. He[3,1,2,a]

[1] Institute of Plasma Physics, Chinese Academy of Sciences, P.O. Box 1126, Hefei 230031, P.R. China
[2] College of Physics Science and Technology, Yangzhou University, Yangzhou 225002, P.R. China
[3] CCAST(World Laboratory), P.O. Box 8730, Beijing 100080, P.R. China

Received 23 April 2003/ Received in final form 13 December 2003
Published online 9 March 2004 –

Abstract. In a kicked rotor subjected to a piecewise-continuous force field, it is observed that a stochastic web and the chaotic diffusion on it suddenly change to transients when an adjustable parameter drives the dissipation. This phenomenon appears to be a new crisis type, which occurs in systems where conservative dynamics may be converted to a dissipative one with a contraction rate showing linear time dependence. It is analytically and numerically shown that, in the crisis, the lifetime dependence obeys universal scaling law suggested by Grebogy, Ott, and Yorke [Phys. Rev. Lett. **57**, 1284 (1986)], and the scaling exponent takes a special value, 1, due to the dissipation characteristics. Additionally presented is another power law that describes, from another viewpoint, the transition of a conservative stochastic web (which is a fat fractal) to a non-attracting thin fractal (the strange repeller).

PACS. 05.45.Ac Low-dimensional chaos

1 Introduction

All the practical systems are dissipative. Selecting evenly many initial points in phase space, their trajectories asymptotically tend to one (or several) subset(s), which is (are) embedded in phase space and addressed "attractor(s)". If an invertible mapping describes the system, the ordinary dissipation expression is that the size of the phase space region occupied by the moving phase points continuously (usually in average exponentially) decreases. The area in phase space, occupied by the initial points (which are attracted by an attractor), is called "basin" of the attractor. If the system is described by a noninvertible mapping, two or more points in phase space iterate to a common image (in certain conditions) that induces a phase space collapse. The effect may be called noninvertibility-induced dissipation, which usually is much weaker (the size of the phase space region occupied by the moving phase points usually in average decreases linearly) than the above-mentioned ordinary dissipation and thus often ignored. This paper will show a situation where this effect exists alone and therefore cannot be ignored. It is then easy to image the situation where the effect exists together with the ordinary dissipation.

In such a conventional dissipative system, when a chaotic trajectory suddenly escapes through a "leaking hole" (which suddenly appears at a control parameter's threshold value and grows continuously from zero size) from a chaotic attractor, so that the attractor suddenly expands, vanishes, or merges into another one, a "crisis" occurs [1–3]. In an everywhere smooth dissipative system, a crisis often happens when the unstable manifold (its closure is the chaotic attractor) of an unstable periodic orbit crosses the stable manifold (its closure is the basin boundary) of itself (or another unstable periodic orbit). The small region between the stable manifold and the unstable manifold forms a leaking hole. Grebogy, Ott, and Yorke discovered and analytically explained this phenomenon and deduced a famous rule showing the power-law dependence of the averaged lifetime, $\langle\tau\rangle$, of the motion in the original chaotic attractor on the driving parameter, ϵ [2]:

$$\langle\tau\rangle \sim \epsilon^{-\nu}, \qquad \text{when} \quad \epsilon \to 0, \tag{1}$$

where ν, the scaling exponent, should take a value of $1/2$ in an one-dimensional case, or a value between $1/2$ and $3/2$ in a two-dimensional case, depending on the unstable periodic orbit's properties [2]. There are only a few observed crises, which do not obey scaling law (1). References [3,4] present two examples. After a crisis, the leaking hole's backward image set removes nearly all the original chaotic attractor's points. The remnants form a fractal set that is addressed as a chaotic saddle (in an invertible system) or a strange repeller (in a noninvertible system) [2,5,6]. Trajectories starting from points of a chaotic saddle or a strange repeller never leave the saddle or repeller and exhibit chaotic motion forever. However, it is completely unlikely to hit such a point by random choice since the saddle

[a] e-mail: drhe@mail.yzu.edu.cn

or repeller is a zero measure set and globally unattractive. What is observable experimentally is not the saddle or repeller itself but rather a small neighborhood of it. Trajectories starting close to the saddle or repeller can stay for a long time in its neighborhood and show chaotic properties, but sooner or later they escape. Thus the chaotic saddle or strange repeller leads to transient chaos. In some systems the chaotic transients may be superlong, and can be addressed as super-transients [7]. Properties of chaotic saddles or strange repellers and chaotic transients are important physical quantities in many practical fields, for example, in controlling chaos [8] and sustaining chaos [9].

Many practical systems frequently show sudden changes. They are often described by piecewise continuous dissipative functions. In these systems, other types of crises may be found, such as a "hole-induced crisis" [4,10] and a "discontinuity-induced crisis" [11]. In recent years, some scientists have paid attention to piecewise continuous conservative systems [12–20]. Among them, Hu, Chen, and their cooperators discussed a system exemplified by a particle in an infinite potential well subject to a periodic kicking force [16,17]. What they are interested in is a kind of two-dimensional map, which is, as shown by equation (2), a concatenation of two sub-maps, f_1 and f_2. Their definition ranges are two subsets, D_1 and D_2, of phase space. The smooth borderline between D_1 and D_2 is called the discontinuity borderline, which is a basic concept in this article

$$\begin{bmatrix} x_{n+1} \\ y_{n+1} \end{bmatrix} = f_1 \begin{bmatrix} x_n \\ y_n \end{bmatrix} \qquad \text{if} \quad (x_n, y_n) \in D_1$$

$$\begin{bmatrix} x_{n+1} \\ y_{n+1} \end{bmatrix} = f_2 \begin{bmatrix} x_n \\ y_n \end{bmatrix} \qquad \text{if} \quad (x_n, y_n) \in D_2. \qquad (2)$$

In the case investigated in references [16,17], the concatenation map is invertible as shown by maps (4) and (5) with $\beta = 1$. Hu et al. found, in this system, a type of diffusion in a stochastic web with special scaling properties [16,17]. It is interesting that the stochastic web is formed by the discontinuity borderline's image set [17] (this is explained in the next section). In references [18,19], the authors studied an electronic relaxation oscillator model and its simplified models. All the models are described by discontinuous concatenations of two conservative sub-maps as shown by equation (2). In certain conditions the discontinuity induces noninvertibility and the aforementioned noninvertibility-induced dissipation, which cannot be ignored since, in this case, the much stronger ordinary dissipation cannot appear. The systems were addressed as quasi-dissipative. In such systems the special weak dissipation should show some influence to the system's behavior. Considering the crisis examples observed in conservative systems [20], it would seem probable to find a crisis with some unique properties in quasi-dissipative systems. Indeed, in reference [21] the authors reported such a crisis. However, they did not discover any unique feature in the lifetime's scaling law, which is the most important crisis property.

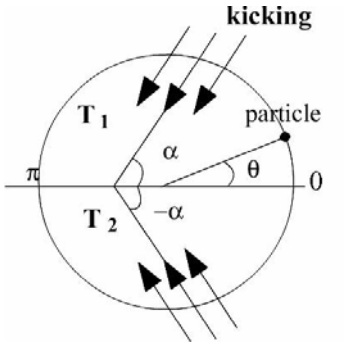

Fig. 1. A schematic showing the system's model.

This article presents a system that is similar to what is discussed in references [16,17]. However, the current system is able to display a continuous transition from a piecewise continuous conservative system to a quasi-dissipative system by adjusting a single parameter. A crisis is observed showing a special value, 1, of the scaling exponent due to its dissipation characteristics. The article is arranged as follows: Section 2 introduces the system and its properties; Section 3 describes the crisis; Section 4 discusses the strange repeller; Section 5 contains a discussion and conclusion.

2 The system

A kicked rotor is a famous physical model displaying important features such as onset of chaos, phase locking, and so on. It can also be used for introducing standard mapping (Chirikov Taylor mapping) [22]. The current study suggests examining a classical particle moving without friction along a unit circle subjected to a periodic impulsive force (of impulse strength K, as shown in Fig. 1). The impulse's periods, T_i $(i = 1, 2)$, are different in the upper (T_1) and lower (T_2) semicircles. Along the tangent direction of the circle, the impulsive forces can be expressed as:

$$\begin{cases} f_1 = K \sin(\theta - \alpha)\delta_{T_1}(t), & (0 < \theta \le \pi), \\ f_2 = K \sin(\theta + \alpha)\delta_{T_2}(t), & (\pi < \theta \le 2\pi), \end{cases} \quad \text{when} \qquad (3)$$

where θ denotes the angular position, α represents the angle between the direction, at which the impulse is applied, and the diameter that connects the two positions of the boundaries, 0 and π, and $\delta_{T_i} = \sum_{n=-\infty}^{\infty} \delta(t - nT_i)$. After a subjection of f_i impulse the next impulse applies only after T_i time duration even if the particle crosses the discontinuity border. This means that the system has a type of "memory", so that the particle may make a free motion in a time duration longer than T_2 in the lower half of the circle if $T_2 < T_1$ and vice versa. For example, if $T_2 = T_1/2$, after last kicking at a position near to the border $\theta = \pi$ in the upper semicircle, the particle will make a free motion in a T_1 time duration even if it moves, after crossing the border, in $\theta \in [\pi, 2\pi]$ longer then $T_2 = T_1/2$.

By integrating the impulse along the tangent direction of the circle and the angular momentum of the moving

particle from just before the nth kick to just before the $(n+1)$th kick, one gets:

$$\begin{cases} \theta_{n+1} = \theta_n + I_{n+1} \pmod{2\pi} \\ I_{n+1} = I_n + k\sin(\theta_n - \alpha), \end{cases} \quad \text{if} \quad (0 < \theta_n \leq \pi), \tag{4}$$

$$\begin{cases} \theta_{n+1} = \theta_n + \beta I_{n+1} \pmod{2\pi} \\ I_{n+1} = I_n + k\sin(\theta_n + \alpha), \end{cases} \quad \text{if} \quad (\pi < \theta_n \leq 2\pi), \tag{5}$$

where $I = pT_1/m$, $k = KT_1/m$, p denotes the momentum along the tangent direction of the circle, m denotes the mass of the particle, and $\beta = T_2/T_1$. When $\beta = 1$, maps (4), (5) become exactly the system presented in reference [17]. The reference shows this system is piecewise continuous conservative and invertible [17]. The following demonstrates that the mappings become noninvertible and quasi-dissipative when $\beta \neq 1$.

It is easily verified that both sub-maps (4) and (5) are area-preserving, and their inverse maps can be deduced easily as:

$$\begin{cases} \theta_n = \theta_{n+1} - I_{n+1} \pmod{2\pi} \\ I_n = I_{n+1} - k\sin(\theta_n - \alpha), \end{cases} \quad \text{if} \quad (0 < \theta_n \leq \pi), \tag{6}$$

$$\begin{cases} \theta_n = \theta_{n+1} - \beta I_{n+1} \pmod{2\pi} \\ I_n = I_{n+1} - k\sin(\theta_n + \alpha), \end{cases} \quad \text{if} \quad (\pi < \theta_n \leq 2\pi). \tag{7}$$

Please note that in order to find an inverse image, (θ_n, I_n), the principal for selecting (6) or (7) depends on the position θ_n instead of θ_{n+1}. This creates the possibility of finding two (θ_n, I_n) points for the same (θ_{n+1}, I_{n+1}) according to the different inverse mapping form. This is the "noninvertibility induced by discontinuity", which is the source of quasi-dissipative property.

3 The crisis of a stochastic web

3.1 The stochastic web

Firstly, consider the case when $\beta = 1$ and maps (4) and (5) become invertible and conservative. There are two discontinuity borderlines in the system function's definition range. The borderlines are denoted by $\{(\theta, I)|_{\theta=0}\}$ and $\{(\theta, I)|_{\theta=\pi}\}$. In phase space the images of the borderlines incline, split and bend continuously during an infinite iteration process so that the image set forms a fractal. In the conservative kicked rotor system ($\beta = 1$), the fractal takes the form of a network as shown in Figure 2. The figure was obtained by recording the first 2000 iterations from evenly distributed 101 initial values of $\{(\theta, I)|_{\theta=\pi, I\in[-0.5,0.5]}\}$. The reason for confining the initial values to the range, $[-0.5, 0.5]$, was only for obtaining a suitable figure size. The parameter values are: $\alpha = 0.2$, $k = 0.4$, and $\beta = 1$.

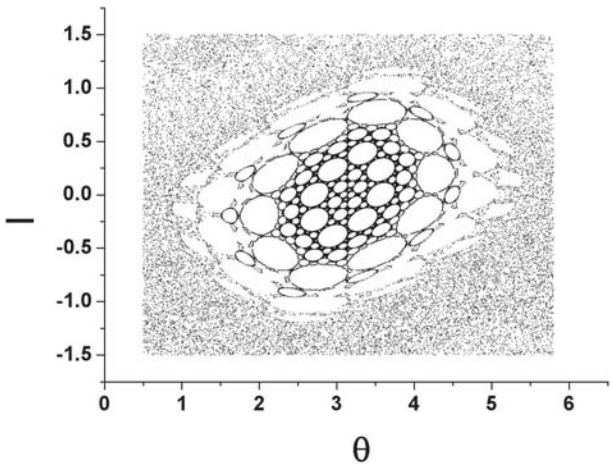

Fig. 2. The stochastic web formed by the images of the discontinuity borderlines. The details are explained in the text.

The numerical investigation confirms that, in the network, iterations perform boundless chaotic diffusion. Therefore, it can be addressed as a stochastic web. It is observable that there are many (actually an infinite number of) holes in the network where elliptic islands are located. Regular motion is restricted in the islands to where chaotic iterations never enter. The backward images of points in the stochastic web are always in the web, and the backward images of points in the islands are always in the islands.

Figure 3 shows the first four images of the borderline $\{(\theta, I)|_{\theta=\pi}\}$ as well as the largest elliptic orbits in some of the elliptic islands inside the web holes to illustrate that the discontinuity borderline's image set forms the stochastic web. The black lines (showing the first four images of the borderline) are drawn by recording the first (indicated by 1 and the small arrow), second (by 2), third (by 3), and fourth images (by 4) of the evenly distributed 101 initial values on $\{(\theta, I)|_{\theta=\pi, I\in[-0.5,0.5]}\}$. The gray dots (showing the largest elliptic orbits in the elliptic islands) are drawn by recording 1000 iterations from suitable initial values, which are selected inside the holes in the center part of the network shown in Figure 2. For clarity we show the first and the fourth images of the borderline in Figure 3a (by thinner or wider black lines, respectively) and the second and third in Figure 3b (also by thinner or wider black lines, respectively). It is obvious that the first image of the borderline only inclines because the borderline belongs to the definition range of map (4) and thus iterates only according to the single nonlinear map function. The situation becomes different later since the first image already crosses the borderline so that the different segments have to iterate according to different mapping functions, (4) or (5). That is why the second image splits in two pieces. Both these two lines cross the borderline therefore the third image splits into four. With similar reason the fourth image splits into six pieces. From the first to the fourth, the higher the image is, the more it bends due to the nonlinear feature of the mapping functions. All segments of the borderline images are tangent to the elliptic islands. It is easy to realize that the infinite

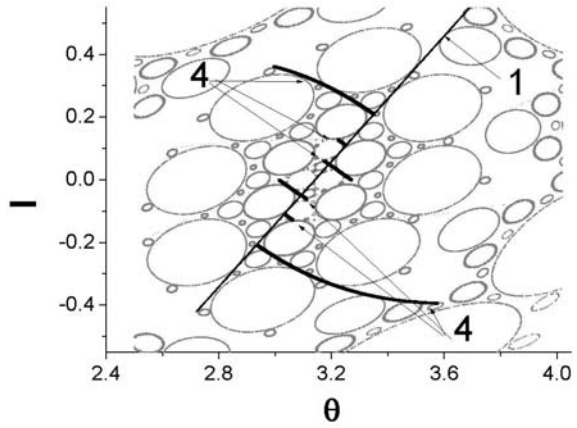

(a)

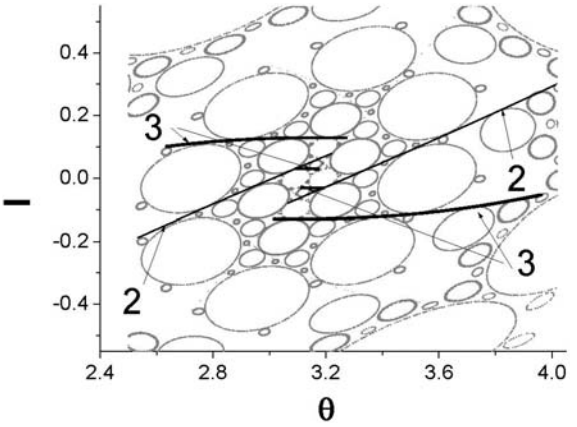

(b)

Fig. 3. The first four images of the borderline $\{(\theta, I)|_{\theta=\pi, I\in[-0.5,0.5]}\}$ and some elliptic islands inside the web. The parameter values are: $\alpha = 0.2$, $k = 0.4$, and $\beta = 1$. The first and the fourth images are shown in (a) (by thinner or wider black lines, respectively). The second and third images are shown in (b) (also by thinner or wider black lines, respectively).

number of the borderline images mainly form the center part of the web where many holes appear as shown in Figure 2. The images of the borderline $\{(\theta, I)|_{\theta=0}\}$ are also tangent to the elliptic islands, but they mainly form the outside part of the web where no holes appear as shown in Figure 2.

3.2 The transient stochastic web and the leaking holes

Maps (4) and (5) become noninvertible and quasi-dissipative when $\beta \neq 1$. The only case discussed here is when $\beta \leq 1$. The situation when $\beta \geq 1$ is basically the same. In this case, a point in the elliptic islands may have two backward images according to different sub-maps (6) or (7), respectively. One of them is still inside the islands and corresponds to conservative motion. Another is outside the islands and should be inside the stochastic web (cf. Fig. 4b). That means there is possibility for the iterations on the web to enter the elliptic islands. Mira has proven analytically that in some kinds of two-dimensional piecewise continuous noninvertible maps, like systems (4) and (5), the chaotic area is bounded by image segments of the discontinuity borderlines [23]. According to the conclusion, the motion on the web should be chaotic, but now it becomes a transient. Sooner or later, it finally escapes from the web via a leaking hole and enters to the islands to perform a conservative regular motion. The leaking hole should be the set of the points on the elliptic islands, which have two backward images. One of them is still inside the islands. Another is inside the stochastic web (cf. Fig. 4b).

The black dots in Figure 4a are drawn by recording the last 1000 iterations after ignoring the first 199000 from each of the 101 initial values evenly distributed on $\{(\theta, I)|_{\theta=\pi, I\in[-0.5,0.5]}\}$. Since no stochastic web is visible, they show that the elliptic island surfaces represented by the dots now attract the points. More specifically, the stochastic web stretches into the islands so that a very thin "ring" on the surface of each elliptic island, which is the intersection between the stochastic web and the island, becomes the leaking hole. The intersection part, the surface ring, is the set of points on the island, which have two backward images (one of the images is inside the transient stochastic web). The parameter values are: $\alpha = 0.2$, $k = 0.4$, and $\beta = 0.98$. In order to obtain a more convictive proof, a ring at the surface of an island in a period-8 elliptic island chain, which is shown in Figure 4a by larger black dots and indicated by "A", is chosen and the following computation has been performed. Choose 16 evenly distributed "diameters" of the ellipse and then select evenly 10001 points on each diameter. Then search if the points have one or two backward images. The results confirm that all the points, which have two backward images (one of them is inside the transient stochastic web), fall in the region inside the surface ring indicated by "A" in Figure 4a. For clarity, Figure 4b shows the leaking hole (the ring which is shown in Fig. 4a), a point on it (which is indicated by A), and the two backward images of A, A_1 and A_2. It is obvious that A_1 is in the transient stochastic web (drawn by recording the iterations from each of the 400×400 initial values evenly distributed on $\{(\theta, I)|_{\theta\in[\pi-1.0,\pi+1.0], I\in[-0.5,0.5]}\}$, which do not enter the leaking holes yet), while A_2 falls in another elliptic island, which belongs to the same period-8 elliptic island chain. The similar computation is performed with two different values of β: 0.85 and 0.60 (the results for $\beta = 0.60$ is shown in Fig. 4c). Also, 18 β values have been chosen evenly in the range $\beta \in [0.94, 0.9994]$. For each β value the computation is performed but the number of the diameters are only 6. All the results convinced us that the leaking holes always take forms of the surface rings (both the external and internal borders of the leaking holes are ellipses). Based on this understanding, we can draw the surface rings (the leaking holes) shown in Figures 4a, 4b and 4c in a more simple and convenient way: choose 1001 points evenly on both the axes of the elliptic island, where the ring is located. Then, select those, which have two backward images. Finally, record the first 1000 iterations from each of these selected initial values.

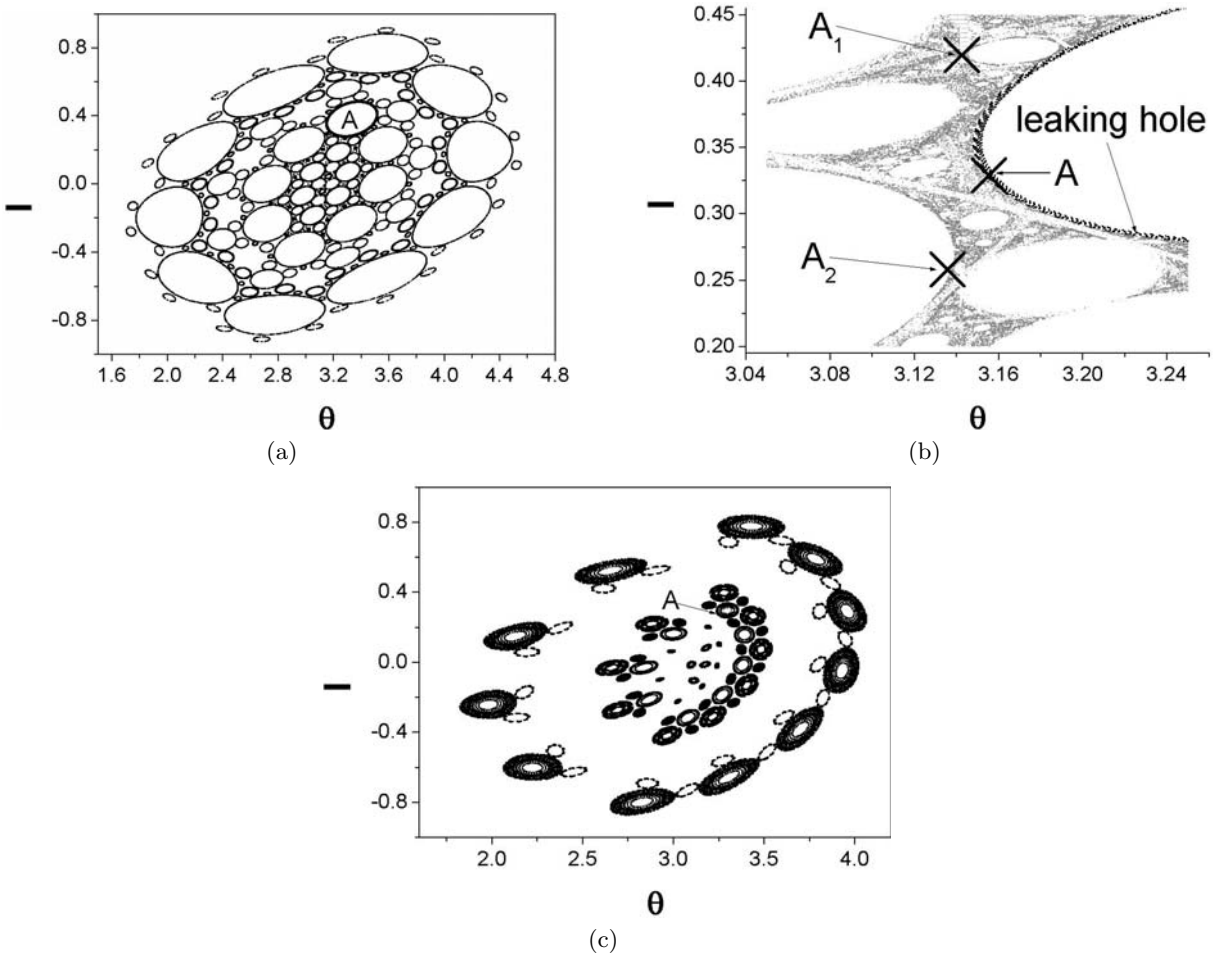

Fig. 4. (a) The leaking holes at the parameter values: $\alpha = 0.2$, $k = 0.4$, and $\beta = 0.98$. (b) A leaking hole shown in (a), a point on it, and the two backward images of the point. (c) The leaking holes at the parameter values: $\alpha = 0.2$, $k = 0.4$, and $\beta = 0.60$. They are drawn by recording the last 1000 iterations after ignoring the first 199000 from each of the 101 initial values evenly distributed on $\{(\theta, I)|_{\theta=\pi, I\in[-0.5,0.5]}\}$. The hole (the ring) indicated by "A" is drawn in a more simple way: choose 1001 points evenly on both the axes of the elliptic island, where the ring is located. Then, select those, which have two backward images. Finally, record the first 1000 iterations from each of these selected initial values. The results show the same ring form like others, which belong to the same elliptic island chain. It is obvious that the rings (the holes) become much wider than those at $\beta = 0.98$ although different rings may have different widths. Please note that each of the 21 small "thin" rings shown in this figure is actually a period-8 island chain. Each of the 8 small spots in it actually is a small ring with similar width.

The numerical investigation also shows the following conclusions. When $\epsilon = \beta - \beta_c$ ($\beta_c = 1$) is small (as the situation shown in Figs. 4a and 4b), the leaking holes (rings) are also small (very thin), and there is a super-long transient chaotic motion before the regular conservative iterations. The length of the transients is strongly dependent on the initial values. In this situation the transient stochastic web almost keeps the same pattern as the original (when $\beta = 1$), however the iterations on it finally escape to many elliptic islands (as demonstrated by Fig. 4a). When $\epsilon = \beta_c - \beta$ becomes increasingly larger, the leaking holes (rings) become increasingly wider (as the situation shown in Fig. 4c), and the transient chaotic motion becomes increasingly shorter. The transient stochastic web gradually loses its network form. The illustration of the transient stochastic web in different β values and the variation of its fractal dimension may also be interesting, but the results are presented elsewhere [24].

3.3 Escape from the transient stochastic web and the rule of the crisis

To signify the gradual escape change from the transient stochastic web, an average lifetime, $\langle\tau\rangle$, is defined as:

$$\langle\tau\rangle = \lim_{n\to\infty} \frac{\sum_{i=1}^{n} \tau_i}{n}, \tag{8}$$

where n denotes the number of initial values and τ_i denotes the number of iterations in the transient stochastic web starting from initial value i. Approximate mathematical descriptions for the leaking holes (the surface

rings) around all the larger elliptic islands have been established, so the iterations in the transient stochastic web (before entering the holes) can be quite precisely determined. The transition from the stochastic web, which exists in $\beta = 1$, to the transient web (when $\beta \leq 1$) can be addressed as a kind of crisis, and the average lifetime can be expected to follow the famous power law rule, which is expressed by (1). Now, following Grebogy, Ott, and Yorke [2], the special phase space contraction rate's (in quasi-dissipative systems) influence on lifetime scaling behavior is considered. If the leaking hole takes an area Δ at a control parameter value ϵ, it is iterated backwards in time for n steps and obtains a region with an area Δ'. In an everywhere smooth and conventionally dissipative two-dimensional map, discussed in reference [2], the measure Δ' depends on an unstable periodic orbit's properties. However, in a quasi-dissipative two-dimensional map, it can simply be predicted that $\Delta' = 2m\Delta$, where $m \leq n$, since it is only in some iterations that two phase space pieces can iterate to one, and the much stronger exponential contraction (which appears in a conventionally dissipative system) is absent. Assuming that the area of the leaking hole, Δ, is proportional to control parameter value, ϵ, and that the probability, $P(\Delta)$, with which the iterations visit the hole, obeys a rule $P(\Delta) \propto \rho\Delta$, where ρ denotes the visiting probability to a unit area in Δ, for the iteration process from Δ' to Δ, one can get:

$$\frac{P(\Delta)}{P(\Delta')} = \frac{\rho\Delta}{\rho\Delta'} = \frac{\epsilon}{2m\epsilon} = \frac{1}{2m}. \tag{9}$$

So, considering the widely accepted assumption $\langle\tau\rangle \sim 1/P(\Delta)$ one gets:

$$\frac{\langle\tau\rangle(\epsilon)}{\langle\tau\rangle(2m\epsilon)} = \frac{\epsilon^{-\nu}}{(2m\epsilon)^{-\nu}} = \frac{1}{(2m)^{-\nu}} = \frac{P(\Delta')}{P(\Delta)} = \frac{1}{(2m)^{-1}}. \tag{10}$$

This means that this crisis, with the assumption, has a special scaling exponent, $\nu = 1$. In the current sample crisis, numerical results confirm that:

$$\Delta \propto \epsilon \tag{11}$$

as shown by Figure 5. Thus the special scaling exponent, $\nu = 1$, should be measured here.

Figure 6 shows numerical results about the relationship between $\langle\tau\rangle$ and the driving parameter $\epsilon = \beta_c - \beta$ ($\beta_c = 1$). The solid linear line on the double logarithmic $\epsilon - \langle\tau\rangle$ plane shows the least square fitting of the data, which crosses 5 magnitude degrees and expresses good agreement with the power scaling law expressed by equation (1). The corresponding variation range of parameter β is 0.968−0.99941. The computation takes much effort because the areas of many regular quasi-attractors in each β value must be distinguished. A result with even higher resolution is very difficult to obtain. The scaling exponent, $\nu = 1.01 \pm 0.03$, agrees very well with the analytic discussion.

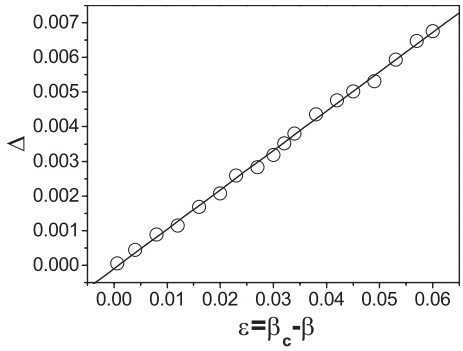

Fig. 5. The numerical results, which show the measure of the leaking hole, Δ, (the area occupied by it in phase space) is proportional to the control parameter, $\epsilon = \beta_c - \beta$. The variation range of β is [0.94, 0.9994]. Note that Δ is dimensionless. The parameter values are: $\alpha = 0.2$, $k = 0.4$.

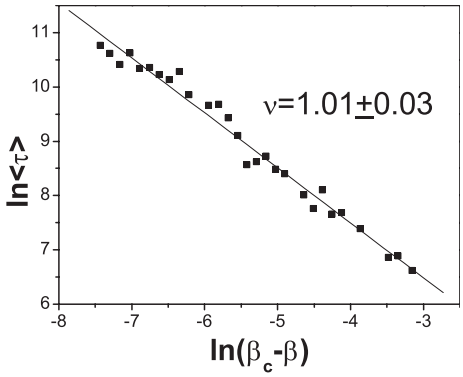

Fig. 6. The relationship between the average lifetime, $\langle\tau\rangle$, and the controlling parameter. The computation methods are indicated in the text. The parameter values are: $\alpha = 0.2$, $k = 0.4$, and $\beta \in [0.968, 0.99941]$.

4 The strange repellers

4.1 The strange repellers in phase space

As stated in the first section, after this crisis, the set of the leaking hole's backward images cuts out nearly all points in the transient stochastic web. The fractal remnants can be defined as a strange repeller. Figure 7 shows a strange repeller that was drawn with the parameter values $\alpha = 0.2$, $k = 0.4$, and $\beta = 0.98$ (same as Fig. 4) in the following way: selecting the initial values with iterations that showed a lifetime 10 times longer than $\langle\tau\rangle$, and then recording the transience (the iterations before entering the leaking holes) which started from them but ignoring the first and last 20%. This method is similar to the "single trajectory method", which was suggested by Tél in 1991 [6]. This simple method works here. Figure 8 shows the computation results for obtaining the repeller's fractal dimension by the box-counting method. In the figure, l denotes the size of the box, the scale. N denotes the number of data-occupied boxes in the scale. The good linear fit means that the pattern shown in Figure 7 is a fractal. The fitting line's slope is the fractal dimension, which is 1.889 ± 0.009.

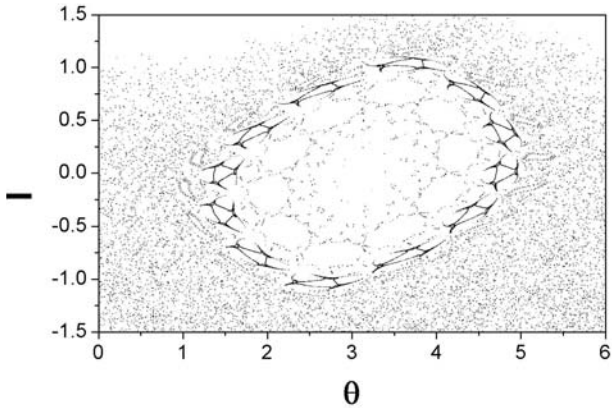

Fig. 7. A strange repeller when $\alpha = 0.2$, $k = 0.4$, and $\beta = 0.98$.

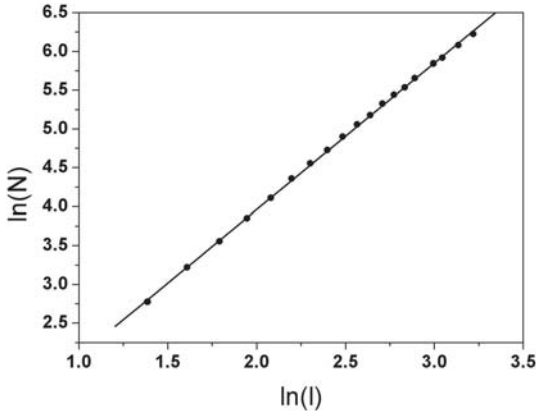

Fig. 8. The computation results for obtaining the fractal dimension of the repeller shown in Figure 7 by the box-counting method. Parameter values are: $\alpha = 0.2$, $k = 0.4$, and $\beta = 0.98$.

When ϵ increases so that the leaking hole becomes larger, the fractal remnants on the transient stochastic web gradually concentrate to the area near to the regular quasi-attractors. The next sub-section describes this phenomenon via the strange repeller's fractal dimension variation.

4.2 The strange repeller's fractal dimension variation

The strange repeller's gradual change may be expressed by a figure that draws the relationship between the repeller's fractal dimension and the driving parameter, ϵ. Figure 9 shows the numerical results, which indicate a rule:

$$D = (0.016 + 0.41\epsilon)^{-0.168}, \tag{12}$$

where $\epsilon = \beta_c - \beta$ ($\beta_c = 1$), and β crosses a wide range, $\beta \in [0.23, 1]$. The repeller's fractal dimension, D, was computed similarly by the box-counting method. When $\epsilon \to 0$, equation (12) leads to a conclusion that $D \to 2$, which is the phase space dimension where the repeller is embedded.

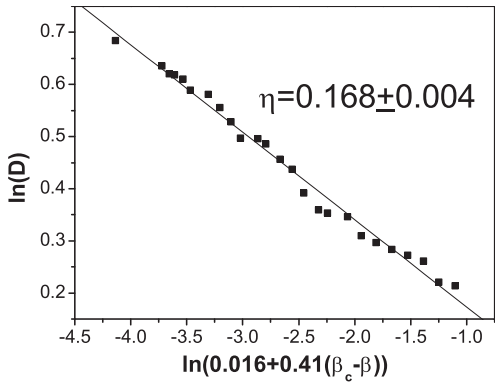

Fig. 9. The relationship between the repeller's fractal dimension, D, and the controlling parameter. The parameter values are: $\alpha = 0.2$, $k = 0.4$, and $\beta \in [0.23, 1]$.

5 Conclusion and discussion

A new crisis type has been observed in a system where continuous variation of parameter, β, can adjust the system's dissipation characteristics, so the area-preserving chaotic diffusion on a stochastic web suddenly changes to a transient. After the crisis, the original conservative system becomes quasi-dissipative, in which the phase space contraction rate is linear instead of exponential (an exponential contraction rate being common in a conventional dissipative system). In the current system, as quantitatively supported, the crisis shows a special lifetime scaling exponent, $\nu = 1$, because the visiting probability to a unit area in the leaking hole does not depend on the control parameter, and the leaking hole's measure is proportional to the control parameter. This should be the most simple and typical case in quasi-dissipative systems. More examples of crises, which show differing scaling exponents in different quasi-dissipative systems, can be observed. After the crisis, a strange repeller (a non-attracting fractal set) can be defined on which iterations make an infinitely long chaotic motion. The numerical results show that the repeller's fractal dimension variation obeys another power law when changing the controlling parameter. This power law leads to an important conclusion that, when the control parameter, ϵ, tends to zero (the critical value of the crisis), the strange repeller's fractal dimension tends to 2, which equals the dimension of the original stochastic web (a fat fractal existing before the crisis). This number also equals the phase space dimension where the repeller is embedded. Therefore, this rule may describe the crisis even better by displaying a sudden transition from a conservative fat fractal stochastic web to a non-attracting thin fractal transient web. Immediately after the crisis, when ϵ is very small, the transient web shows a fractal dimension very near to 2 (the fractal dimension of the original fat web), and a network form very similar to that of the original fat web. As ϵ increases, the transient web's fractal dimension gets continuously smaller and gradually loses the network form.

This study is supported by the National Natural Science Foundation of China under Grant No. 10275053. The authors would like to thank Professor Kangjie Shi at Northwest University, China for the very helpful discussion and suggestions.

References

1. C. Grebogi, E. Ott, J.A. Yorke, Phys. Rev. Lett. **48**, 1507 (1982); Physica D **7**, 181 (1983)
2. C. Grebogi, E. Ott, J.A. Yorke, Phys. Rev. Lett. **57**, 1284 (1986); C. Grebogi, E. Ott, F. Romeiras, J.A. Yorke, Phys. Rev. A **36**, 5365 (1987)
3. C. Grebogi, E. Ott, J.A. Yorke, Phys. Rev. Lett. **50**, 935 (1983); Ergod. Theor. Dynam. Sys. **5**, 341 (1985)
4. S.-X. Qu, B. Christiansen, D.-R. He, Acta Phys. Sin. **44**(6), 841 (1995) (*in Chinese*)
5. H.E. Nusse, J.A. Yorke, Physica D **36**, 137 (1989)
6. T. Tél, in *Directions in Chaos*, edited by B.-L. Hao, D.-H. Feng, J.-M. Yuan (World Scientific, Singapore, 1991), Vol. 3
7. Y.-C. Lai, R.L. Winslow, Phys. Rev. Lett. **74**, 5208 (1995)
8. E. Ott, C. Grebogi, J.A. Yorke, Phys. Rev. Lett. **64**, 1196 (1990); D. Auerbach, C. Grebogi, E. Ott, J.A. Yorke, Phys. Rev. Lett. **69**, 3479 (1992)
9. Y.-C. Lai, C. Grebogi, Phys. Rev. E **49**, 1094 (1994)
10. S.-X. Qu, B. Christiansen, D.-R. He, Phys. Lett. A **201**, 413 (1995)
11. X.L. Ding, S.G. Wu, Y.C. Yin, D.R. He, Chin. Phys. Lett. **16**, 167 (1999)
12. I. Dana, N.W. Murray, I.C. Percival, Phys. Rev. Lett. **62**, 233 (1989)
13. F. Borgonovi, G. Casati, B. Li, Phys. Rev. Lett. **77**, 4744 (1996)
14. F. Borgonovi, Phys. Rev. Lett. **80**, 4653 (1998)
15. F. Borgonovi, P. Conti, D. Rebuzzi, B. Hu, B. Li, Physica D **131**, 317 (1999)
16. B. Hu, B. Li, J. Liu, Y. Gu, Phys. Rev. Lett. **82**, 4224 (1999)
17. H.-S. Chen, Jiao Wang, Y. Gu, Chin. Phys. Lett. **17**, 85 (2000)
18. J. Wang, X.-L. Ding, B. Hu, B.-H. Wang, J.-S. Mao, D.-R. He, Phys. Rev. E **64**, 026202 (2001)
19. J. Wang, X.-L. Ding, B.-H. Wang, D.-R. He, Chin. Phys. Lett. **18**, 13 (2001)
20. Y.-C. Lai, C. Grebogi, R. Blumel, I. Kan, Phys. Rev. Lett. **71**, 2212 (1993); Y.-C. Lai, C. Grebogi, Phys. Rev. E **49**, 3761 (1994)
21. X.-M. Wang, Y.-M. Wang, K. Zhang, W.-X. Wang, H. Chen, Y.-M. Jiang, Y.-Q. Lu, J.-S. Mao, D.-R. He, Eur. Phys. J. D **19**, 119 (2002)
22. G.M. Zaslavsky, R.Z. Sagdeev, D.A. Usikov, A.A. Chernikov, *Weak Chaos and quasi-regular patterns* (Cambridge Univ. Press, Cambridge, 1991), p. 47
23. C. Mira, Inter. J. Bifur. Chaos **6**, 893 (1996)
24. Y. Jiang, Y. Lu, D.-R. He, Acta Phys. Sin. **53**(2), 383 (2004) (*in Chinese*)